AMERICAN SOCIETY FOR MICROBIOLOGY | mBio®

RESEARCH ARTICLE

Transient Glycolytic Complexation of Arsenate Enhances Resistance in the Enteropathogen *Vibrio cholerae*

Emilio Bueno,[a] Víctor Pinedo,[a] Dhananjay D. Shinde,[b] André Mateus,[c] Athanasios Typas,[c] Mikhail M. Savitski,[c] Vinai C. Thomas,[b] Felipe Cava[a]

[a]Laboratory for Molecular Infection Medicine Sweden, Department of Molecular Biology, Umeå Centre for Microbial Research, Umeå University, Umeå, Sweden
[b]Center for Staphylococcal Research, Department of Pathology and Microbiology, University of Nebraska Medical Center, Omaha, Nebraska, USA
[c]Genome Biology Unit, European Molecular Biology Laboratory (EMBL), Heidelberg, Germany

ABSTRACT The ubiquitous presence of toxic arsenate (As^{V}) in the environment has raised mechanisms of resistance in all living organisms. Generally, bacterial detoxification of As^{V} relies on its reduction to arsenite (As^{III}) by ArsC, followed by the export of As^{III} by ArsB. However, how pathogenic species resist this metalloid remains largely unknown. Here, we found that *Vibrio cholerae*, the etiologic agent of the diarrheal disease cholera, outcompetes other enteropathogens when grown on millimolar concentrations of As^{V}. To do so, *V. cholerae* uses, instead of ArsCB, the As^{V}-inducible *vc1068-1071* operon (renamed *var* for vibrio arsenate resistance), which encodes the arsenate repressor ArsR, an alternative glyceraldehyde-3-phosphate dehydrogenase, a putative phosphatase, and the As^{V} transporter ArsJ. In addition to Var, *V. cholerae* induces oxidative stress-related systems to counter reactive oxygen species (ROS) production caused by intracellular As^{V}. Characterization of the *var* mutants suggested that these proteins function independently from one another and play critical roles in preventing deleterious effects on the cell membrane potential and growth derived from the accumulation As^{V}. Mechanistically, we demonstrate that *V. cholerae* complexes As^{V} with the glycolytic intermediate 3-phosphoglycerate into 1-arseno-3-phosphoglycerate (1As3PG). We further show that 1As3PG is not transported outside the cell; instead, it is subsequently dissociated to enable extrusion of free As^{V} through ArsJ. Collectively, we propose the formation of 1As3PG as a transient metabolic storage of As^{V} to curb the noxious effect of free As^{V}. This study advances our understanding of As^{V} resistance in bacteria and underscores new points of vulnerability that might be an attractive target for antimicrobial interventions.

IMPORTANCE Even though resistance to arsenate has been extensively investigated in environmental bacteria, how enteric pathogens tolerate this toxic compound remains unknown. Here, we found that the cholera pathogen *V. cholerae* exhibits increased resistance to arsenate compared to closely related enteric pathogens. Such resistance is promoted not by ArsC-dependent reduction of arsenate to arsenite but by an operon encoding an arsenate transporter (ArsJ), an alternative glyceraldehyde 3-phosphate dehydrogenase (VarG), and a putative, uncharacterized phosphatase (VarH). Mechanistically, we demonstrate that *V. cholerae* detoxifies arsenate by complexing it with the glycolytic intermediate 3-phosphoglycerate into 1-arseno-3-phosphoglycerate (1As3PG). 1As3PG is not transported outside the cell; instead, it is subsequently dissociated by VarH to enable extrusion of free arsenate through ArsJ. Collectively, this study proposes a novel mechanism for arsenate detoxification, entirely independent of arsenate reduction and arsenite extrusion, that enhances *V. cholerae* resistance to this metalloid compared to other enteric pathogens.

KEYWORDS arsenate, arsenite, enteric pathogens, Transposon-seq, *Vibrio cholerae*

Arsenic is a toxic metalloid commonly found in aquatic and terrestrial environments (1–3) as arsenate (As^{V}) or its reduced form, arsenite (As^{III}). The potent toxicity of this element makes it one of the best-studied natural poisons that impact public health

Invited Editor Andrew J. Roe, University of Glasgow

Editor Edward G. Ruby, University of Hawaii at Manoa

Address correspondence to Felipe Cava, felipe.cava@umu.se, or Emilio Bueno, emilio.bueno@umu.se.

The authors declare no conflict of interest.

Received 9 June 2022
Accepted 22 August 2022
Published 14 September 2022

(4). The mechanism of As^V toxicity is due to its structural resemblance to phosphate oxyanions and its uptake into the cell through phosphate transport channels (5, 6). Once in the cytoplasm, As^V can replace phosphate in energy-generating reactions, resulting in the formation of ADP-As^V instead of ATP by the ATP synthase and through substrate-level phosphorylation during glycolysis (7, 8). Conversely, cellular toxicity by As^{III} is exerted by a different mechanism. As^{III} can interact directly with thiol groups of proteins and other molecules, thereby interfering with diverse cellular processes (9, 10). Despite its risk to public health, arsenic has been used as an antimicrobial agent to treat infectious diseases (1, 4, 11, 12), increasing the selective pressure for microbes to acquire arsenic resistance.

Bacterial strategies to resist As^V include chelation by metal-binding metallothioneins (13), methylation to less toxic and more volatile arsenic derivatives (14), respiration (15), and extrusion of As^V or As^{III} by specific efflux pumps (e.g., ArsJ and ArsB, respectively) (9, 16–18). In bacteria, the most common mechanism of As^V resistance genes occurs via As^V reduction to As^{III}, followed by the extrusion of the latter through an As^{III} transporter (19). As^V resistance genes are commonly organized in operons, e.g., the *arsRDABC* operon from *Escherichia coli* R773 (19). In this example, *arsC* encodes a dedicated arsenate reductase, and *arsB* encodes an efflux pump of As^{III} (20). The *arsR* gene encodes the repressor of the *ars* operon. When As^{III} is present, its interaction with ArsR releases it from the *ars* promoter, thus increasing transcription of the operon. *arsA* encodes an ATPase that, together with ArsB, forms the As^{III} extrusion system. Alternatively, As^{III} extrusion via ArsB can be driven by proton motive force in bacterial species lacking ArsA. Finally, *arsD* encodes a chaperone that enhances arsenic extrusion by transferring As^{III} to ArsAB (9).

Despite being extensively studied in environmental soil and marine bacterial species, the mechanisms underlying As^V resistance in human-pathogenic bacteria remain largely unknown. Here, we investigated As^V resistance in representative enteric pathogens and found that *Vibrio cholerae* exhibits remarkably high resistance to this metalloid. Using genome mining and functional characterization, we demonstrated that *V. cholerae* does not detoxify As^V by reducing it to As^{III}. Instead, transposon-based functional screens identified the operon *vc1068-1071* as the primary genetic determinant of As^V resistance in *V. cholerae*. Mechanistic characterization of this system revealed that resistance to As^V in *V. cholerae* is mediated by a transient metabolic complexation of As^V with the glycolytic intermediate 3-phosphoglycerate (3PG) to generate 1-arseno-3-phosphoglycerate (1As3PG). Our results support that this As^V-containing metabolite is transient in the cell: its formation cushions the cellular damage caused by free As^V, while its dissociation enables *V. cholerae* to release free As^V through the ArsJ efflux permease.

RESULTS

High resistance to arsenate in *V. cholerae* is independent of the ArsC reductase. While studying the tolerance of enteropathogenic bacteria to metalloids, we observed that *Vibrio cholerae*, the causative agent of cholera, was able to grow in media supplemented with supraphysiological (30 mM) concentrations of arsenate (As^V) (see Fig. S1 In the supplemental material). This level of resistance was unmatched by other human enteric pathogens, as lower concentrations of As^V (10 mM) readily caused total or partial growth inhibition of *Salmonella enterica*, *Citrobacter rodentium*, *Yersinia pseudotuberculosis*, enterohemorrhagic *E. coli* (EHEC), and *Shigella flexneri* (Fig. 1A). Consistently, *V. cholerae* outcompeted these species by 5- to 500-fold in coculture experiments grown in media supplemented with As^V (Fig. 1B).

To investigate the molecular mechanisms of As^V resistance in *V. cholerae*, we first searched for canonical determinants for As^V detoxification in its genome. *V. cholerae vc2165* encodes a homolog of *E. coli* K-12 arsenate reductase ArsC, including the conserved catalytic cysteine and arginine residues (21, 22) (Fig. S2A). However, while *E. coli*'s ArsC enzyme is critical for resistance to As^V, inactivation of *vc2165* did not compromise

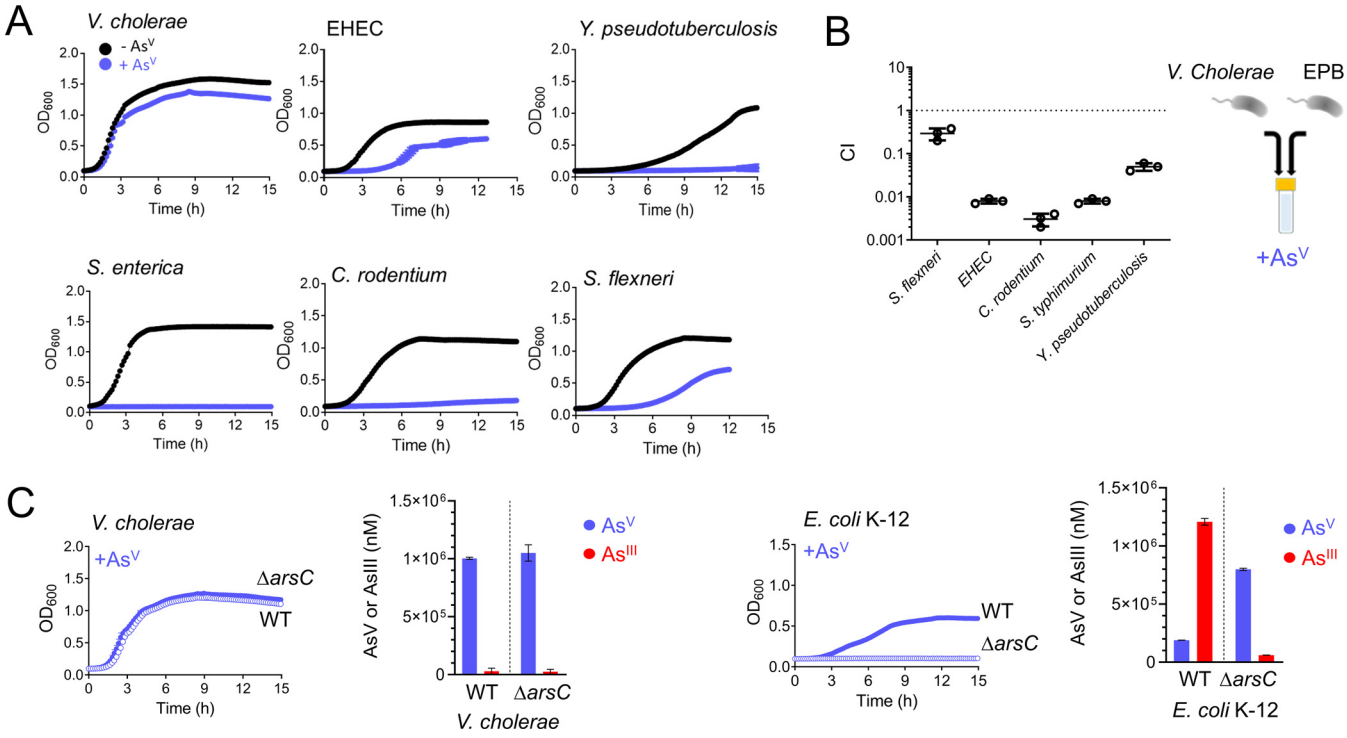

FIG 1 *V. cholerae* is the enteric pathogen with the greatest resistance to As^V. (A) Growth curves (OD_{600}) of the enteric pathogens *V. cholerae*, enterohemorrhagic *Escherichia coli* (EHEC), *Salmonella enterica*, *Citrobacter rodentium*, *Shigella flexneri*, and *Yersinia pseudotuberculosis*. Cultures were grown in LB medium in the absence (black) and in the presence (blue) of 10 mM arsenate (As^V). (B) *In vitro* competition among *V. cholerae* and other enteropathogenic bacteria (EPB) studied in panel A. Cells were incubated in LB medium supplemented with 10 mM As^V for 8 h. CI values from competition in the presence of As^V were normalized with respect to CI values in the absence As^V. (C) Growth curves (OD_{600}) of WT (blue filled circles) and *arsC* (blue empty circles) mutant strains from *V. cholerae* and *E. coli* K-12. Cultures were grown in LB medium supplemented with 10 mM As^V. As^V and As^{III} concentrations were determined by ICP-MS from supernatants of *V. cholerae* and *E. coli* WT and *arsC* mutant strains after 8 h of incubation in 1.5 mM As^V. Data are the mean of three biological replicates ± the standard error of the mean (SEM).

V. cholerae growth in the presence of this metalloid (Fig. 1C). Thus, we reasoned that *V. cholerae*'s ArsC might not be active or expressed. To measure ArsC activity, we quantified extracellular As^V and As^{III} by inductively coupled plasma mass spectrometry (ICP-MS) and observed that while *E. coli* reduced ~80% of As^V to As^{III} in an ArsC-dependent manner, *V. cholerae* produced no As^{III} (Fig. 1C). Interestingly, replacement of the *V. cholerae arsC* allele by that of *E. coli* caused growth inhibition, likely due to toxic As^{III} formation, as growth was recovered by expressing *E. coli*'s As^{III}-transporter, ArsB (Fig. S2B). Altogether, these results indicate that *V. cholerae* ArsC is inactive and that As^V resistance in this bacterium is independent of the ArsC-ArsB system that relies on the production and elimination of As^{III}.

Resistance to As^V in *V. cholerae* depends on the *vc1068-vc1071* operon. To identify the genetic determinants conferring resistance to As^V in *V. cholerae*, we performed two complementary genome-wide screenings based on (i) transposon insertion sequencing (TIS) and (ii) the use of a previously described *V. cholerae* transposon mutant library (23) (Fig. 2). Both screens permit assessment of the mutants' relative fitness. While screening of the *V. cholerae* transposon mutant library assesses fitness of individual mutants in separated wells, TIS valuates subtle fitness differences during growth under competition with other mutants from the Tn-library. In TIS, a *V. cholerae* transposon library containing ~500,000 mutants is generated and incubated in parallel with and without AsV (see representation in Fig. 2). Transposon Q absent after incubation with AsV indicate the essentiality of those determinants to survive under such condition.

Only four nonessential Transposon mutants (*vc1068*::*tn*, *vc1069*::*tn*, *vc1070*::*tn*, and *vc1071*::*tn*) were mutually underrepresented in both screenings (Fig. 2). We renamed *vc1068-71 var* for *vibrio* arsenate resistance cluster for reasons described below. *vc1068* encodes a homolog of the ArsR repressor, *vc1069* (renamed *varG*) encodes a putative glyceraldehyde-3-phosphate dehydrogenase (GAPDH), *vc1070* (renamed *varH*) encodes

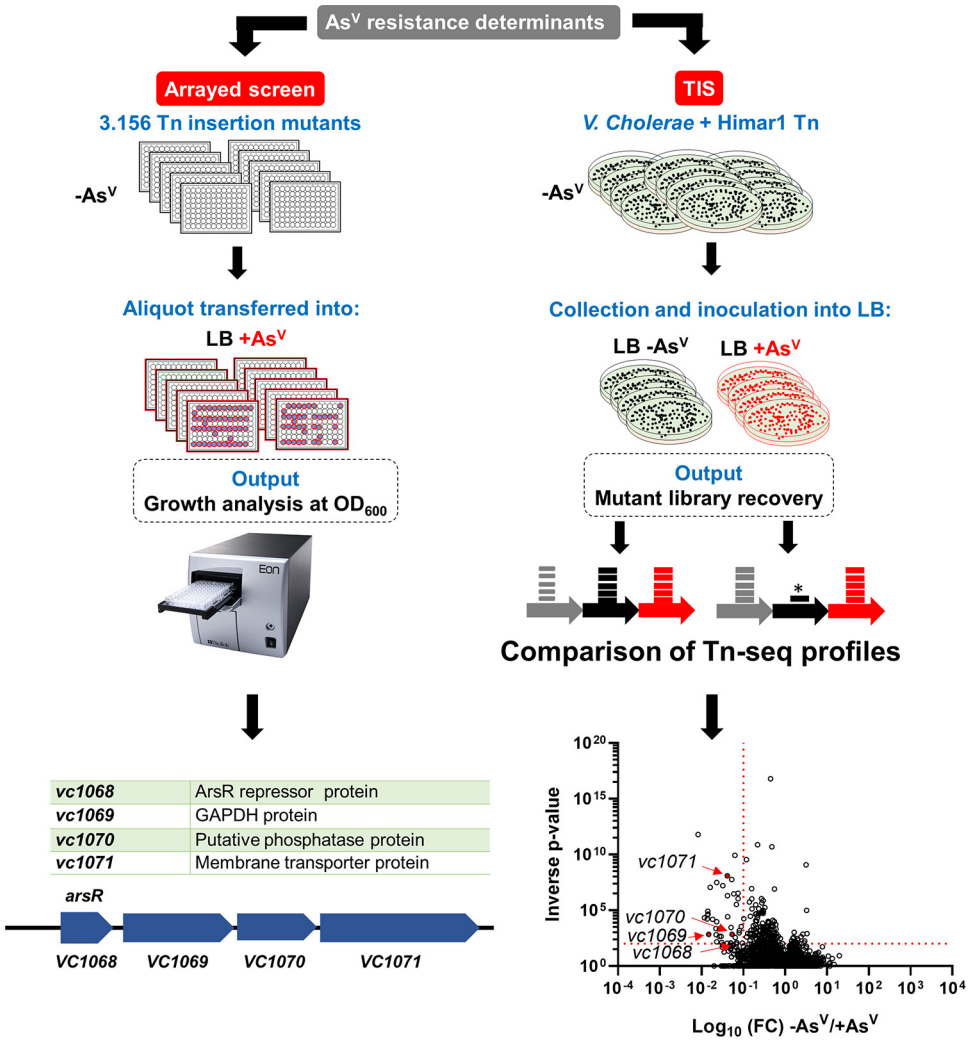

FIG 2 Identification of essential genetic determinants for As^V resistance in *V. cholerae*. (Left) Experimental workflow for an arrayed transposon mutant screen to identify the genes required for As^V resistance in *V. cholerae* and the list of mutant strains identified. (Right) Experimental workflow for TIS screen in the presence and absence of 1 mM As^V. Volcano plot depicting the ratio of read counts mapped to individual genes in transposon libraries of (*V. cholerae* plated onto medium supplemented with As^V). Red dotted lines indicate arbitrary thresholds of a fold change of (FC) <0.1 and an inverse *P* value of >20. Genes in red show loci also identified in the arrayed screen (see Table S1 for an extended version).

an uncharacterized putative phosphatase, and *vc1071* encodes an ArsJ-like As^V transporter (17). As expected, the *arsC* mutant was not identified in the screens, confirming that *V. cholerae* does not detoxify As^V by reducing it to As^{III}. Although homologues to VarG and ArsJ were previously reported in *Pseudomonas aeruginosa*, their function in As^V resistance has not been studied *in vivo* (17).

To verify the implication of the *var* cluster on As^V resistance, we constructed individual in-frame markerless deletion mutants. All mutants were sensitive to As^V except for Δ*arsR* (Fig. 3A), suggesting that the conditional lethality of the *arsR*::tn was likely due to the polar effect on the expression of the downstream genes *varG*, *varH*, and *arsJ*. Indeed, transcriptional analysis using fusions of the *lacZ* reporter to potential promoter regions located upstream of each *var* gene demonstrated that expression of this cluster depends on As^V, and it is driven from a single promoter upstream of *arsR* (Fig. S3). Inactivation of *arsR* turned transcription from this promoter constitutive (in both the presence and absence of As^V), confirming that VC1068 is the *V. cholerae* ArsR repressor of the *var* operon (Fig. S3). Further characterization revealed that Δ*arsJ* presents a

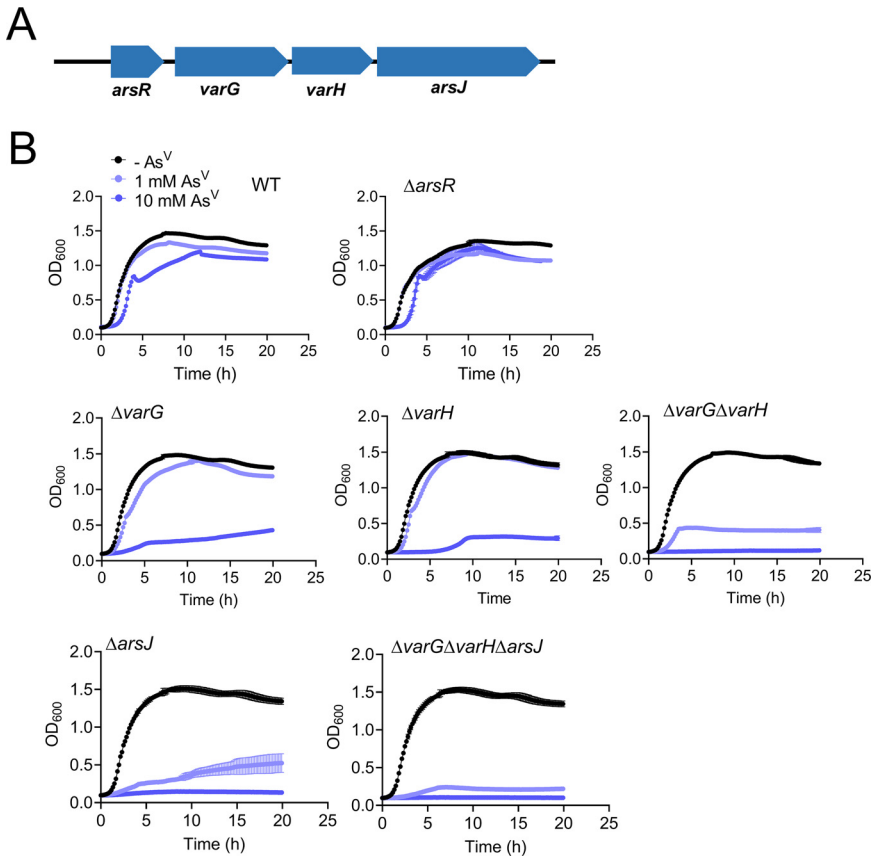

FIG 3 Phenotypic characterization of the *V. cholerae var* operon. (A) Var operon. (B) Growth curves (OD_{600}) of *V. cholerae* WT, single, and combinatorial *var* mutant strains. Cultures were grown in LB medium in the absence or presence of 1 and 10 mM As^V. Data are the mean of three biological replicates ± SEM.

more dramatic growth defect than the rest of the *var* mutants at low As^V concentrations (1 mM) (Fig. 3). However, at 10 mM As^V, the growth of the *varG* and *varH* mutant strains was also compromised despite the presence of ArsJ. These results suggest that the ArsJ transporter is the main determinant for As^V resistance in *V. cholerae*, but VarG and VarH also become relevant at higher concentrations of As^V. Furthermore, the inactivation of *varG*, *varH*, and *arsJ* (double and triple mutants) aggravated growth defects exhibited by the single mutants, suggesting complementary/synergistic functions for these proteins in As^V resistance in *V. cholerae* (Fig. 3A).

VarG is an As^V-inducible GAPDH that preferentially binds As^V. *V. cholerae* VarG presents a high degree of protein sequence (E value, 5^{e-86}) (Fig. S4A) and structure (AlphaFold2 TM-score, 0.96) (Fig. S4B), similar to the glycolytic GAPDH VC2000 (Gap), including the conserved catalytic Cys residue (24). To characterize VarG's activity compared to the glycolytic paralogue Gap in particular, we purified both proteins from *V. cholerae* and performed *in vitro* GAPDH activity assays (25) in the presence or absence of As^V. While both proteins exhibited GAPDH activity, VarG showed preference for As^V over P_i (the canonical substrate) (Fig. 4A). Conversely, the glycolytic GAPDH Gap performed better with P_i. Furthermore, while the expression of *Gap* remained low and constitutive, transcription from the *var* promoter was strongly induced by As^V (Fig. 4B). Therefore, these results suggest that while *V. cholerae* Gap is active on As^V, this enzyme-specific activity and the protein levels are likely insufficient to replace VarG essentiality in *V. cholerae* resistance to As^V.

Arsenate detoxification in *V. cholerae* is facilitated by extrusion of free arsenate instead of being complexed as 1-arseno-3-phosphoglycerate. A VarG homolog from *P. aeruginosa* was proposed to function as a GAPDH that complexes As^V with

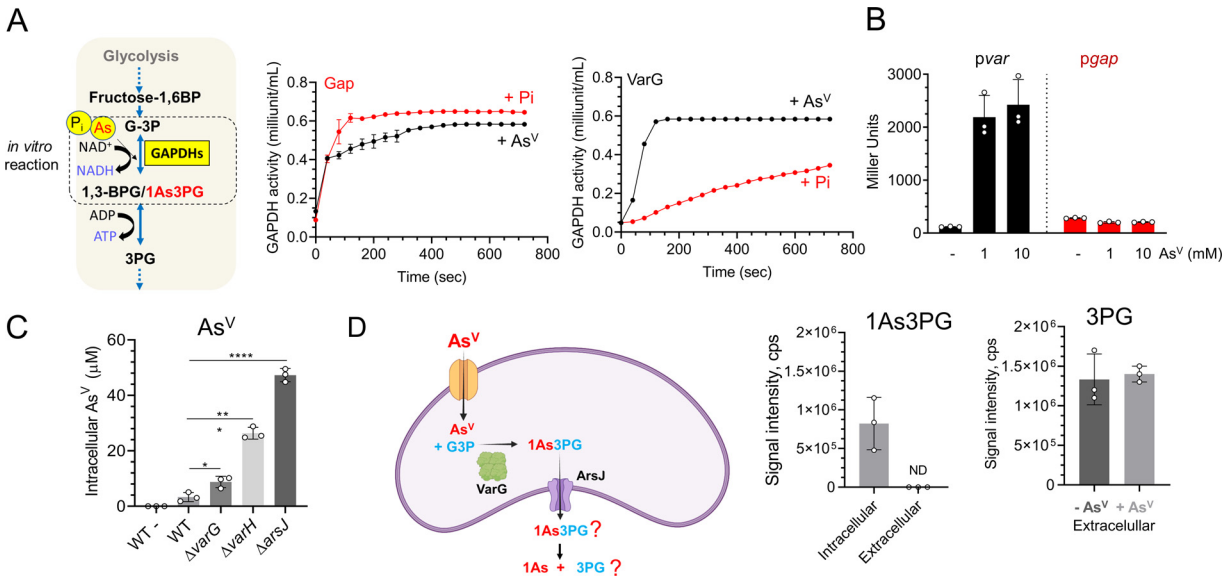

FIG 4 Characterization of *V. cholerae* VarG. (A) *In vitro* GAPDH activity (OD_{450}) of purified *V. cholerae* VarG and the glycolytic Gap enzymes using P_i or As^V as the substrate. (B) β-galactosidase activity of strains in which the *lacZ* reporter gene is cloned under the control of the *var* operon and the *gap* gene promoters. Cultures were grown in LB medium in the absence or presence of 1 and 10 mM As^V for 5 h. (C) Intracellular As^V concentrations of WT, *varG*, *varH*, and *arsJ* mutant strains grown with 1 mM As^V by ICP-MS. (D) (Left) As^V detoxification model in *P. aeruginosa* DK2 (1). (Right) Quantification of 1As3PG and 3PG from intracellular and extracellular samples of *V. cholerae* cells grown with and without 1 mM As^V. Data are the mean of three biological replicates ± SEM.

glyceraldehyde-3-phosphate (G3P) into 1-arseno-3-phosphoglycerate (1As3PG), which is further eliminated through ArsJ (17). However, these experiments were performed *in vitro* using a commercial glycolytic GAPDH from rabbit instead of the As^V-specific GAPDH from *P. aeruginosa* DK2. If this model applies to *V. cholerae*, the absence of either VarG or ArsJ will similarly affect AsV export and resistance. However, our data show that Δ*varG* did not phenocopy the growth defect of Δ*arsJ* (Fig. 3). Furthermore, analysis of intracellular levels of As^V by ICP-MS revealed that, in relation to the wild type (WT), while the Δ*varG* strain only showed moderate (ca. 3×) accumulation of As^V, inactivation of ArsJ accumulated this metalloid ca. 20× (Fig. 4C). Although these results suggest that VarG is not essential to export As^V, we cannot dismiss the possibility of As^V being complexed and extruded as 1As3PG in *V. cholerae*.

Using high-resolution mass spectrometry (HRMS), we detected a mass (*m/z*) of 304.8696 Da, specific to the cultures supplemented with As^V, which was compatible with 1As3PG (*m/z* 304.8674, *m/z* $<$ 0.003 Da difference between experimental and theoretical mass) (Fig. 4D and Fig. S5). 1As3PG was also detected in Δ*varG*, consistent with the ability of the constitutively expressed glycolytic Gap GAPDH to use As^V (Fig. S5). 1As3PG was detected in intracellular cytoplasmic fractions but not in the extracellular milieu, suggesting that this molecule is not expelled in *V. cholerae* (Fig. 4D and Fig. S5). As it has been reported that 1As3PG is rapidly dissociated to As^V and 3PG (26), we reasoned that if exported, its decomposition should increase extracellular 3PG levels in relation to cultures without As^V. However, we found no significant differences in the levels of extracellular 3PG between conditions, supporting the idea that As^V detoxification likely occurs through the release of free As^V rather than 1As3PG through ArsJ (Fig. 4C and Fig. S5).

VarH is involved in 1As3PG dissociation and arsenate export. To find clues that help us understand the role that 1As3PG plays in *V. cholerae*'s resistance to As^V, we investigated VarH. Structural *in silico* analysis using the phyre2 tool (www.sbg.bio.ic.ac.uk/phyre2) and AlphaFold2 revealed that VarH is a cysteine-based protein tyrosine phosphatase (PTP) belonging to the dual-specificity phosphatase superfamily that presents a very high topology similarity to the human Kap PTP phosphatase (Fig. S6A

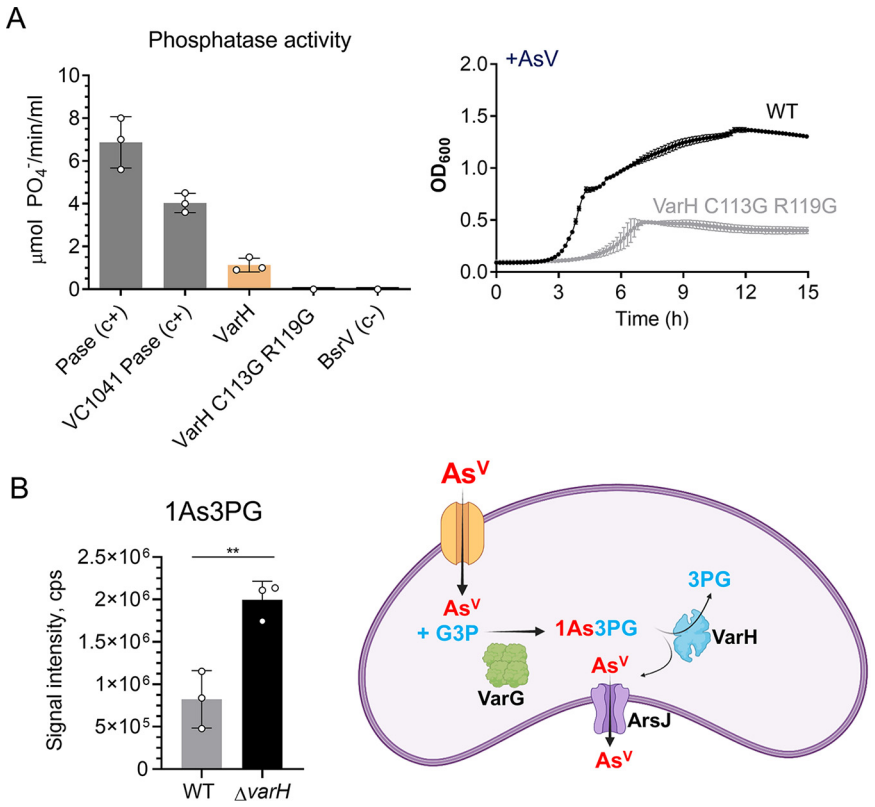

FIG 5 Characterization of *V. cholerae* VarH. (A) (Left) *In vitro* phosphatase activity of purified *V. cholerae* VarH and catalytic mutant derivative where cysteine 113 and arginine 119 were replaced by glycine. *V. cholerae* protein-tyrosine-phosphatase (VC1041) and broad-spectrum racemase (BsrV) were used as positive and negative controls, respectively. (Right) Growth curves (OD_{600}) of *V. cholerae* WT and a VarH catalytic mutant derivative. Cultures were grown in LB medium in the presence of As^V. (B) (Left) Intracellular 1As3PG concentrations from *V. cholerae* WT and Δ*varH* cells grown with and without 1 mM As^V by HRMS. (Right) Schematic of putative mechanism for As^V detoxification in *V. cholerae*. Data are the mean of three biological replicates ± SEM.

and B). To determine if VarH has phosphatase activity, we purified this protein and assessed its capacity to dephosphorylate the chromogenic substrate pNPP. Our results show that, compared to the wheat phosphatase or *V. cholerae*'s PTP VC1041 positive controls, VarH presents lower phosphatase activity, which turned off upon replacement of the putative catalytic cysteine and arginine by glycine residues (Fig. 5A, left panel). Furthermore, consistent with the importance of these residues in VarH activity, replacement of the WT *varH* allele by the catalytically inactive variant *varH* C113G/R119G impaired *V. cholerae* growth in the presence of As^V (Fig. 5A, right panel). These results suggest that the phosphatase activity of VarH is required to provide As^V resistance in *V. cholerae*.

Since VarG and VarH are coregulated by As^V and both support resistance to this metalloid, we hypothesized that VarH could regulate VarG activity by modulating its phosphorylation state. To assess such a possibility, we purified VarG from *V. cholerae* WT and Δ*varH* (Fig. S6C) and analyzed VarG phosphorylation by liquid chromatography-tandem mass spectrometry (LC-MS/MS). However, even though VarG was phosphorylated on Tyr108 and Ser204, those phosphorylation levels were independent of VarH (Fig. S6D). Then, we reasoned that as P_i and As^V are analogs, VarH could potentially act on 1As3PG as a phosphatase to produce 1AsG + Pi or as an "arsenatase" to render 3PG + As^V. Remarkably, we found that 1As3PG concentrations were significantly elevated in Δ*varH* compared to those in the WT strain (Fig. S6E), suggesting that VarH might use 1As3PG as a substrate. Although we could not confirm VarH's activity *in vitro*, potentially due to the instability of 1As3PG (27), the fact that VarH is an active

phosphatase but 1AsG is not detected in *V. cholerae* suggests that VarH could dissociate the 1As3PG complex into 3PG and free As^V, which would be released through ArsJ.

Intracellular arsenate impacts the *V. cholerae* proteome and leads to ROS accumulation and membrane potential defects. To broadly assess global responses triggered by As^V in *V. cholerae*, we analyzed the pathogen proteome upon exposure to As^V. Interestingly, a relatively low number of proteins (~20 proteins) were upregulated upon exposure to As^V, indicating that adaptations to this metalloid might not require extensive proteome rewiring in *V. cholerae*. As expected, these proteins included the As^V resistance Var proteins but also amino acid permeases, a Zn/Cd transporter, members of the phosphotransferase system (PTS)-fructose system, the starvation stress response protein RaiA, and the cysteine synthesis and the peroxiredoxin PrxA (Fig. 6A and B). Cysteine is one of the main targets of reactive oxygen species (ROS) and a functional component of glutathione, which plays a crucial role in the adjustment of cellular redox potential (28). In this line, PrxA has been involved in the adaptation to hydrogen peroxide in *V. cholerae* (29). Therefore, we reasoned that the *var* mutants, which display increased As^V intracellular levels, might suffer from higher oxidative stress than the *V. cholerae* WT strain. To test this hypothesis, we measured ROS levels by analyzing fluorescence of a DNA dye (CellROX green) that emits fluorescence when it is oxidized by ROS in the *V. cholerae* WT and *var* mutant strains and observed a direct correlation between As^V accumulation and ROS level (Δ*arsJ* > Δ*varH* > Δ*varG* > WT) (Fig. 6C). These findings collectively indicate that AsV induces oxidative stress in *V. cholerae*, which is exacerbated in the *var* mutants due to a supraphysiological accumulation of this toxic metalloid.

In addition to ROS affecting Cys-containing proteins, we cannot dismiss a direct effect of As^V on the proteome of *V. cholerae*. To this end, we performed thermal proteome profiling (TPP), a method that globally analyzes multiple types of protein interactions (30). TPP data showed an increased thermal stability of multiple cytosolic proteins that could potentially interact with As^V (~3-fold) in the *var* mutants with respect to the WT (Fig. 6D and Table S1). As^V-interacting protein candidates included proteins involved in the synthesis of heme groups of respiratory cytochromes, respiratory ubiquinone, fermentation, and carbon catabolism, suggesting that accumulation of As^V in Var-defective strains might interfere with cell bioenergetics. To investigate this possibility, we monitored the bacterial membrane potential in the presence of As^V using flow cytometry (Fig. 6E). Interestingly, inactivation of the *var* system resulted in a significant depolarization of the mutant's membrane. Together, these results demonstrate that AsV can, directly and indirectly, affect the *V. cholerae* proteome, leading to oxidative stress and defects in cellular bioenergetics, both possibly related to the growth impairment of the *var* mutants.

The *V. cholerae var* operon provides As^V resistance to enteric pathogens. *In silico* analysis showed that, except for *C. rodentium*, ArsR is the only As^V resistance determinant conserved between *V. cholerae* and the As^V-sensitive enteric pathogens (Fig. 7A). In general, these enteropathogenic species detoxify As^V via ArsC-dependent reduction to As^{III} and subsequent extrusion through ArsB. As *V. cholerae* lacks the As^{III}- production/extrusion tandem ArsCB, we wondered whether the *var* genes could also augment resistance to As^V in other species or would, rather, require additional species-specific elements. To address this question, we expressed the *var* operon excluding the ArsR repressor in enteropathogens sensitive to As^V and studied their growth capacity in the presence of As^V. Strikingly, induced coexpression of *varG-varH-arsJ* in several enteropathogens boosted their growth on As^V (Fig. 7B), demonstrating that the Var system is sufficient and compatible with the ArsCB system in providing resistance against As^V in other bacteria.

DISCUSSION

Arsenic is ubiquitous in the environment due to natural geologic processes and environmental pollution (31, 32). Consequently, most living organisms, including bacteria, encode arsenic resistance proteins (23, 33–37). However, functional characterization of these systems and how they support bacterial fitness in environments with As^V is underappreciated. In this study, we describe that *V. cholerae* exhibits higher resistance to As^V than other enteric pathogens.

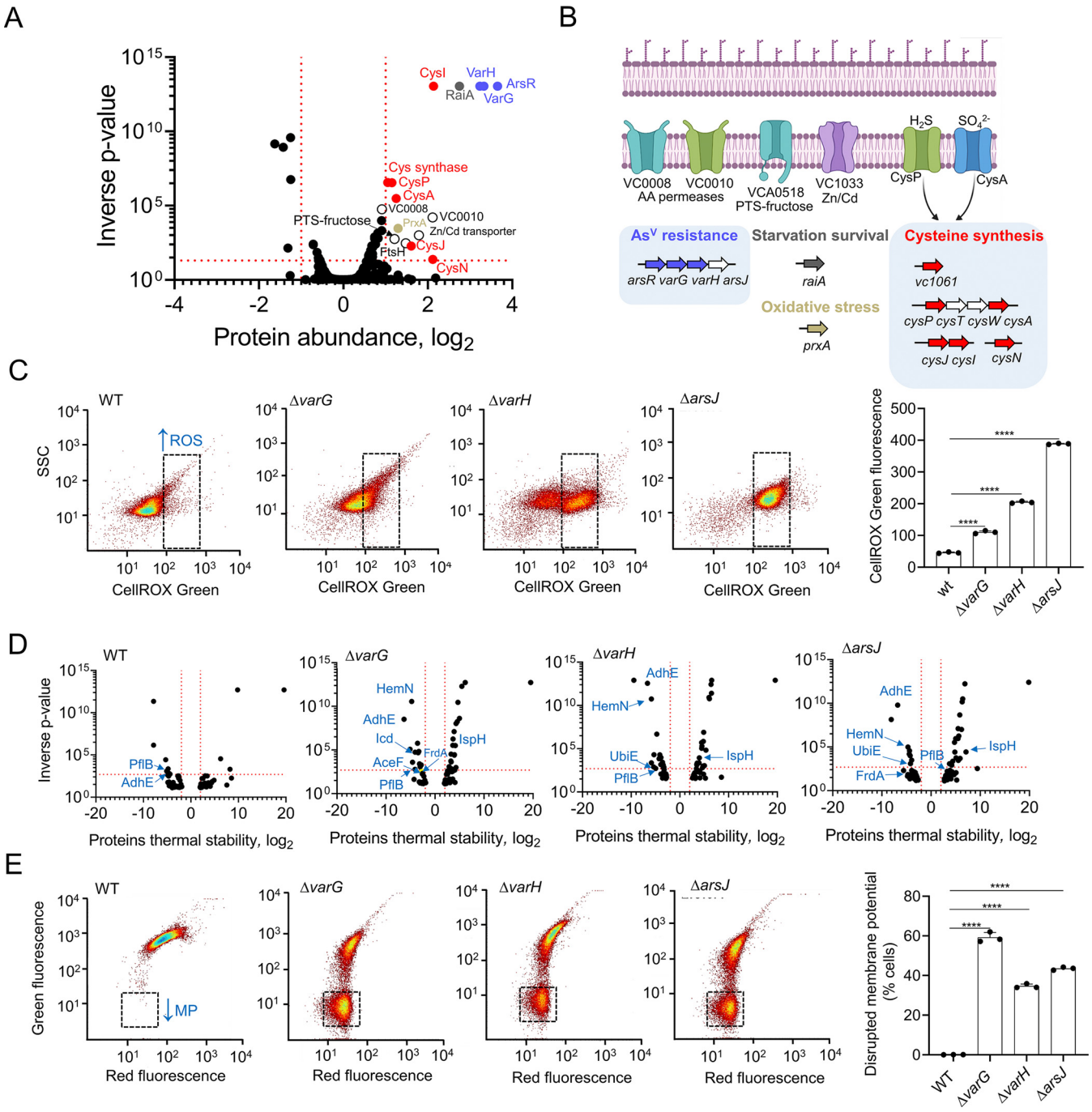

FIG 6 Oxidative stress response and membrane potential alterations of *V. cholerae* WT and the *var* mutants. (A) Volcano plot of LIMMA analysis output depicting read fold change (log_2) of protein abundance and inverse *P* value for each protein queried in the proteomic screen in response to 1 mM As^V in *V. cholerae* WT. Red dotted lines indicate arbitrary thresholds of a fold change (log_2) of >1 or <1 and an inverse *P* value of >20. Var proteins are labeled in blue and oxidative stress related proteins (cysteine biosynthesis and PrxA are labeled as in described in panel B). (B) Schematic of the systems induced in response to As^V in *V. cholerae*. White coloured genes depict undetected genes within an operon. (C) Representative dot plots from *V. cholerae* WT and *var* mutant cells stained with CellRox green following growth in the presence of 1 mM As^V for 5 h. The black dotted gate indicates an area with higher CellRox fluorescence (higher ROS levels). (D) Volcano plot of LIMMA analysis output depicting the read fold change (log_2) of protein thermal stability and inverse *P* value for each protein queried in the proteomic screen in response to 1 mM As^V in *V. cholerae* WT and *var* mutant strains. As^V interacting proteins related to energy-generating pathways are labeled in blue. PflB, VC1866 formate acetyltransferase; AdhE, VC2033 alcohol dehydrogenase/acetaldehyde dehydrogenase; HemN, VC0116 oxygen-independent coproporphyrinogen III oxidase; Icd, VC1141 isocitrate dehydrogenase; FrdA, VC2656 fumarate reductase; IspH, 4-hydroxy-3-methylbut-2-enyl diphosphate reductase; AceF, VC2413 pyruvate dehydrogenase, E2 component; UbiE, VC0083 ubiquinone/menaquinone biosynthesis methyltransferase. (E) Representative dot plots from *V. cholerae* WT and *var* mutant cells stained with DiOC2 following growth in the presence of 1 mM As^V for 5 h. The black dotted gate indicates an area with lowered green fluorescence (lower membrane potential). Data are the mean of three biological replicates ± SEM.

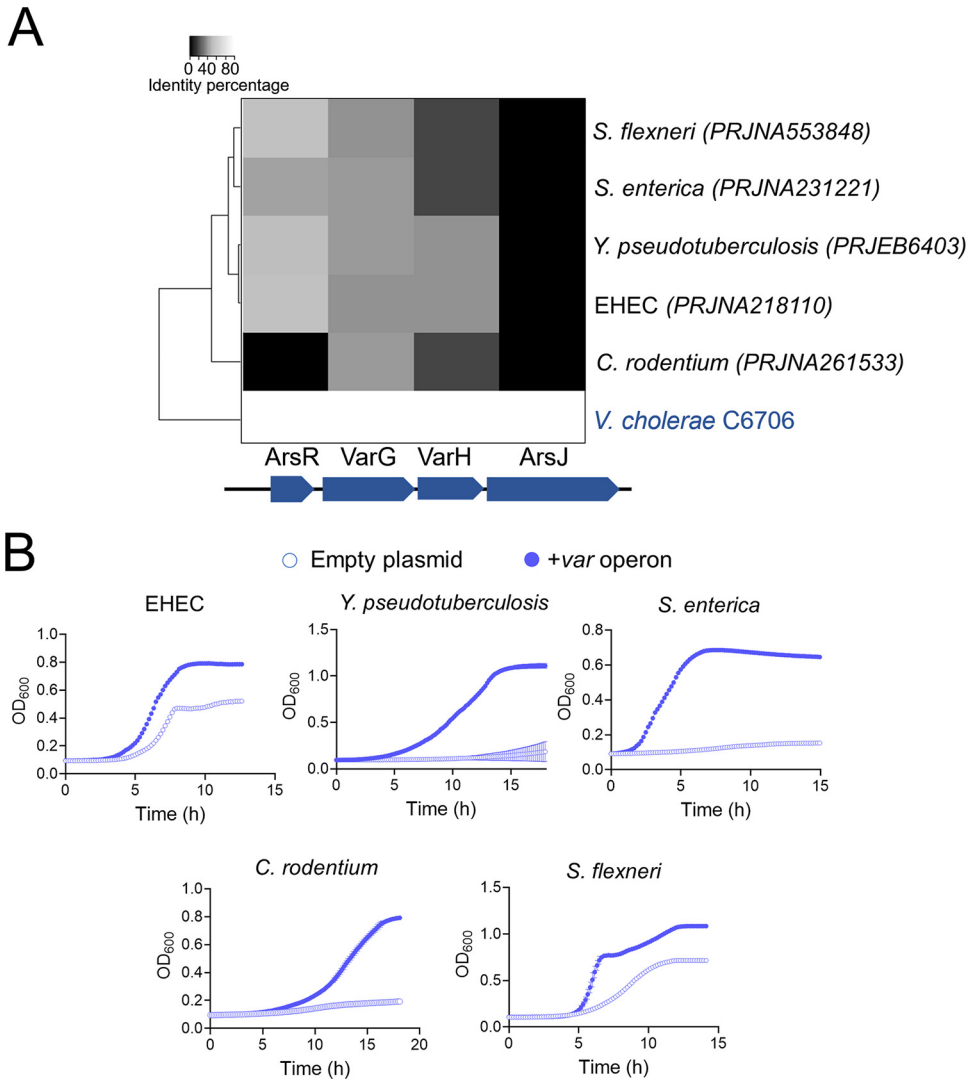

FIG 7 *V. cholerae* Var enhances As^V resistance in enteropathogenic bacteria. (A) Hierarchical heat map clustering of enteropathogenic bacteria with respect to *V. cholerae* based on the percentage identity of *var* genes. (B) Growth curves (OD_{600}) of the As^V-sensitive enteropathogenic bacteria clustered in panel A, carrying an inducible empty plasmid (empty circle) or the same plasmid expressing the *V. cholerae var* operon (blue filled circle). Cultures were grown in LB medium in the presence of 10 mM As^V. Data from panel B are the mean of three biological replicates ± SEM.

The strategy used by *V. cholerae* to resist As^V is different from that used by other gammaproteobacterial enteropathogens. While most of these species encode an ArsC arsenate reductase and an ArsB arsenite efflux pump, *V. cholerae* lacks the latter and has an inactive ArsC. Therefore, *V. cholerae* does not reduce As^V to expel it out of the cell. From an evolutionary perspective, this could be a vestige of a functional ArsCB system that, after losing the ArsB component, has inactivated ArsC to prevent the generation of highly toxic As^{III}. It remains to be investigated whether *V. cholerae* ArsC has undergone functional diversification to fulfill another role in the cell, perhaps related to its neighboring hypothetical genes (*vc2164-vc2167*).

Our screening identified a four-gene operon (*var* operon) conferring resistance to *V. cholerae* that encoded the ArsR repressor, the As^V permease ArsJ, a putative GAPDH (VarG), and a phosphatase (VarH). Interestingly, while most ArsR derepress transcription by sensing As^{III} (38), the lack of As^{III} production in *V. cholerae* suggests that ArsR probably senses As^V in this bacterium. Although more research is required to determine ArsR responses to As^V and As^{III} in *V. cholerae*, comparative sequence analysis between *V. cholerae* ArsR and that of As^{III}-producing bacteria have revealed variations

in conserved residues, including the E→K and C→A substitutions in the As^{III} binding motif (38) (Fig. S7A).

Although GAPDH enzymes are mostly known for their role in glycolysis, they have been functionally linked to diverse processes such as autophagy, oxidative stress responses, apoptosis, posttranscriptional gene regulation, maintenance of DNA integrity, intracellular membrane trafficking, etc. (39–41). A previous study reported that the GAPDH homolog to *V. cholerae*'s VarG detoxified As^V by generating 1As3PG from G3P. However, such conclusions were drawn from *in vitro* experiments that used commercial glycolytic GAPDH from rabbits instead of the specific As^V-inducible GAPDH and monitored As^V transport instead of direct 1As3PG detection (17). Our results, combining *in vitro* GAPDH activity assays and HRMS analyses from intracellular samples provided direct evidence that VarG is a GAPDH that preferentially uses As^V over P_i to synthesize 1As3PG. The role of VarG in *V. cholerae*'s As^V resistance adds to this growing list of GAPDH moonlighting functions.

Although the same study suggested that As^V is exported through ArsJ as 1As3PG (17), the more severe growth defect of *V. cholerae*'s *arsJ* compared to the *varG* mutant suggests that 1As3PG does not play a major role in the export of As^V in this bacterium. Accordingly, the *arsJ* mutant accumulates intracellular As^V ca. 6 times more than the *varG* mutant. Even if we cannot wholly discount the transport of 1As3PG through ArsJ (as this compound can nonetheless be produced in the absence of VarG, likely by the constitutive glycolytic Gap activity), the fact that we have not detected extracellular 1As3PG or increased 3PG in cultures supplemented with As^V suggests that ArsJ expels free As^V.

During glycolysis, the GAPDH enzyme catalyzes the simultaneous phosphorylation and oxidation of G3P to form 1,3 bi-phosphoglycerate (1,3-BPG), which is further converted into 3PG by phosphoglycerate kinase coupled to the transfer of the high-energy phosphate to ADP, making ATP. We reasoned that while the metabolic complexing of As^V into 1As3PG might decrease its toxicity by reducing As^V interaction with *V. cholerae*'s proteome (Fig. 4D), the formation of 1As3PG could be a dead-end product that would affect a major energy-producing pathway. In line with this reasoning, our results showed that VarH presents low phosphatase activity compared to canonical phosphatases. As a low catalytic rate has been previously associated with enzymatic promiscuity (42), we hypothesized that the putative phosphatase VarH would function as an arsenatase that dissociates the 1As3PG complex to clear the glycolytic pathway and free As^V for its export through ArsJ. Indeed, inactivation of VarH results in increased intracellular levels of 1As3PG, which correlates with the accumulation of arsenate in the cell, thereby supporting the idea that ArsJ primarily exports free As^V in *V. cholerae*. Although synteny analyses suggest coevolution between ArsJ and VarG, the presence of VarH is rather exclusive to the *Vibrionaceae* (Fig. S7B). It remains to be investigated whether the amino acid differences in ArsJ between $VarG^+$ and $VarG^-$ species explain the choice of transporting free or complexed As^V.

It has been previously reported that arsenic induces the production of ROS in the cell (43–45). Our results show that in the presence of As^V, *V. cholerae* induces oxidative stress responses, i.e., elevated levels of the hydrogen peroxide-tolerance determinant PrxA (46) and multiple proteins involved in the synthesis of cysteine. As cysteine-containing proteins are targets of ROS (47), and cysteine is also the building block of glutathione, stimulating its synthesis might help to alleviate oxidative damage provoked by As^V. Additionally, we found that As^V directly or indirectly (via ROS) alters the stability of proteins implicated in energy-generating pathways such as Tricarboxylic acid cycle (TCA), fermentation, and respiration. Indeed, As^V accumulation in the *var* mutant dissipated the cellular membrane potential (a proxy of the cell's energy status). The correlation between As^V accumulation with ROS and membrane depolarization exhibited by the *var* mutants suggests that oxidative stress and energy depletion might account for their growth impairment in As^V.

V. cholerae is a pathogenic bacterium endemic to Bangladesh and India, regions where the concentrations of As^V in water and soil are the highest worldwide, in some

areas exceeding concentrations of 1 mM arsenic (48, 49). Hence, *V. cholerae*'s superior resistance to As^V could have evolved as an adaptive strategy to thrive in As^V-rich environments while endowing the cholerae pathogen with a fitness advantage over free-living and host-associated neighboring bacteria. Interestingly, despite the phylogenetic distance, heterologous expression of the *var* operon enhanced As^V resistance in all the pathogens assayed, demonstrating that this system has a high degree of versatility to work in combination with other arsenic detoxification systems.

Collectively, this work proposes a novel mechanism for As^V detoxification in *V. cholerae* that is entirely independent of As^V reduction and As^{III} extrusion. Our results support a model in which the formation of a transient As^V-containing glycolytic intermediate cushions the impact of free As^V in the cell. While a metabolic sink might temporarily aid cells in enduring As^V toxicity, this strategy may exert a high cost in the long term, as glycolysis is a major pathway in cell bioenergetics. We propose that "dearsenylation" of 1As3PG by VarH provides a double benefit by decongesting any jam that may occur in glycolysis and freeing As^V for extrusion to the extracellular medium by ArsJ.

The essentiality of the *V. cholerae var* operon to survive in environments with As^V (such as the host, where concentrations of 100 ppm As^V can be reached [50]) suggests that this machinery may be considered a novel class of bacterial target suitable for therapeutic intervention.

MATERIALS AND METHODS

Bacterial strains and growth conditions. The strains used in this work are listed in Table S2. The *V. cholerae* strains used in this study are derivatives of the El Tor clinical isolate C6706. In addition to *V. cholerae*, this study also used the strains *Escherichia coli* K-12 MG1655 and the *arsC*::Transposon mutant strain from the Keio collection (51), enterohemorrhagic *Escherichia coli* EHEC O157:H7, *Salmonella enterica* serovar Typhimurium LT2, *Citrobacter rodentium* DBS100, *Shigella flexneri* M90T, and *Yersinia pseudotuberculosis* YPIII. Strains were grown aerobically at 37°C in 15-mL tubes containing 3 mL of complete LB medium (10 g tryptone, 10 g NaCl, and 5 g yeast extract/L). To grow *Shigella flexneri*, TSB medium was used (tryptone [pancreatic digest of casein], 17 g soytone [peptic digest of soybean], 3 g glucose, 2.5 g sodium chloride 5 g dipotassium phosphate 2.5). When used, Casamino Acids were supplemented at 1%. To study resistance to As^V, 3×10^6 overnight-grown cells were inoculated into 200 μL of LB medium with or without As^V at the indicated concentrations in 96-well plates, and optical density (OD) values were measured every 10 min using a BioTek Epoch 2 plate reader. Where appropriate, antibiotics were added to *V. cholerae* and *E. coli* cultures at the following concentrations: 200 (streptomycin, Sm), 100 (carbenicillin, Cb), 5 (chloramphenicol, Cm), and 50 μg/mL (kanamycin, Km).

Construction of plasmids to create *V. cholerae* mutants, overexpression constructs, and transcriptional fusions. *V. cholerae* mutants were created by allelic exchange with the suicide plasmid pCVD442 (52). Upstream and downstream DNA fragments (ca. 1 kbp) flanking each coding region were PCR-amplified with the primers listed in Table S3. Upstream and downstream DNA fragments were spliced together by overlapping PCR. The resulting ca. 2-kb fragments were digested as indicated in Table S3 and cloned into pCVD442. For allelic exchange of *V. cholerae arsC* by *E. coli arsC*, a similar protocol was followed, but in this case the *V. cholerae* upstream and downstream DNA regions of *V. cholerae arsC* were spliced together with the *E. coli arsC* gene by overlapping PCR (see Tables S2 and S3). Constructs were transformed into *E. coli* DH5α λpir for amplification. They were confirmed by sequencing, transformed into the *E. coli* donor strain SM10 λpir, and conjugated for 6 h at 37°C with *V. cholerae* C6706 by mixing equal volumes (1 mL) of exponential-phase cultures and spot-plating. Single crossover *V. cholerae* organisms were selected on LB plates with Sm and Cb. Restreaked single colonies were then plated on salt-free LB agar containing 10% (wt/vol) sucrose and Sm. Colonies were streaked on carbenicillin plates to confirm loss of pCVD442 and were then checked by PCR for successful deletion mutants.

Overexpression of *V. cholerae* and *E. coli* genes was carried out by using the arabinose-inducible expression vectors pBAD33 and pBAD18,and the IPTG (isopropyl-β-D-thiogalactopyranoside)-inducible expression vector pHL100 (53) (see Table S2 for specific constructs used for each enteropathogen). To construct each overexpressing plasmid, gene open reading frames including ribosome binding sites were PCR amplified (see primers used in Table S3), double digested with the indicated restriction enzymes, and cloned into each plasmid. Constructs were transformed into the indicated strain by electroporation.

For construction of the transcriptional reporter fusions, gene promoter regions of target genes were amplified using the primers pairs indicated in Table S3. The PCR product was double digested with HindIII and EcoRI and then ligated into HindIII-EcoRI-digested pCB192N (54). Cloned plasmids were then transformed into *V. cholerae* by electroporation.

Purification of recombinant VarG, VC2000, VC1041, and VarH. *V. cholerae* VarG, VC1041, and VarH proteins were overexpressed using the *E. coli* strain BL21 as 6× His-tagged enzymes from a pET28b vector. Overnight cultures were diluted into 250 mL LB broth and grown until an OD at 600 nm (OD_{600}) of 0.5. Flasks were supplemented with 1 mM IPTG and shaken at 37°C for 2 h. Cells were pelleted and resuspended in equilibration buffer (50 mM Tris, pH 7.5, 50 mM NaCl, with protease inhibitor cocktail [Roche]) and disrupted by passaging once through a French press. Lysates were then centrifuged for 1 h

(25,000 rpm, Beckman Coulter Avanti J26-XP centrifuge, JL-25.50 rotor) at 4°C. Nickel-NTA resin (0.5 mL resuspended in equilibration buffer) was then added to the supernatant, followed by incubation at 4°C in a rotating wheel. The lysate was separated from the resin by centrifugation for 1 min at 3,220 × *g*, and the resin was washed (5 × 10 mL) with washing buffer (equilibration buffer adjusted to 1 M NaCl) and eluted with 2 mL of washing buffer containing 500 mM imidazole. Fractions were subjected to SDS-PAGE and Coomassie brilliant blue staining for purity assessment. Protein concentration was quantified with a Bradford assay.

Proteomic and thermal proteome profiling (TPP). We performed TPP to determine protein abundance and thermal stability changes in WT and *var* mutant strains upon exposure to As^V similarly to what was previously described (30, 55). Briefly, WT and mutant cells grown to an OD_{578} of 0.5 were incubated with 1 mM arsenate (or a similar volume of water) for 10 min. Cells were then washed with 10 mL phosphate-buffered saline (PBS) (for cells treated with arsenate, 1 mM arsenate was included in the wash step) and aliquoted to a PCR plate. Each aliquot was then exposed to a different temperature in the range of 37 to 66.3°C for 3 min. Following a 3-min incubation at room temperature, cells were lysed with lysis buffer (final concentration, 50 μg mL^{-1} lysozyme, 0.8% NP-40, 1× protease inhibitor [Roche], 250 U mL^{-1} benzonase, and 1 mM $MgCl_2$ in PBS) for 20 min, followed by three freeze-thaw cycles. Lysates were then prepared for analysis by mass spectrometry by digesting proteins using a modified solid-phase-enhanced sample-preparation (SP3) protocol (56), labeling peptides with TMTpro (Thermo Fisher Scientific) and pooling samples from the same temperature together. These samples were then fractionated to six fractions with high-pH fractionation and injected on an Orbitrap Q-Exactive Plus instrument (Thermo Fisher Scientific) coupled to liquid chromatography (details on the run conditions and instrument parameters as described in Mateus et al. (30, 55)).

Mass spectrometry raw data were searched against the *V. cholerae* FASTA file (UP000000584, downloaded from UniProt) using the Mascot 2.4 (Matrix Science) search engine and isobarquant (57). Protein abundance and thermal stability changes were determined using Limma (58) using the same algorithm as in Mateus et al. (55).

Phosphorylation state of VarG. To identify the VC1069 GAPDH phosphorylation state, *V. cholerae* wild-type and Δ*varH* strains carrying the overexpression vector pHL100 containing the *varG*-HIS tagged gene clone were grown in the presence of As^V and with IPTG. Cells were pelleted, disrupted, and loaded and run in SDS-PAGE gel. VarG-HIS bands were excised and diluted with NuPAGE LDS sample buffer (Invitrogen, Carlsbad, CA) mixed with 10 mM dithiothreitol (DTT) and incubated at 56°C for 20 min, followed by addition of iodoacetamide (IAA) to a final concentration of 20 mM. The sample was loaded on 4 to 12% NuPAGE (Invitrogen). The electrophoresis was run in MOPS (morpholinepropanesulfonic acid) buffer at 180 V for 1 h. The gel was stained with Coomassie brilliant blue. Bands of interest were cut from the SDS-PAGE. The bands were digested with trypsin, followed by identification using liquid chromatography-tandem mass spectrometry (LC-MS/MS). MS/MS spectra were searched with Proteome Discoverer 2.3 (Thermo Fisher Scientific) against the two sequences obtained for phosphate groups (UniProtKB). The precursor tolerance and fragment tolerance were set to 10 ppm and 0.05 Da, respectively. Trypsin was selected as the enzyme, and methionine oxidation, phosphorylation of serine, tyrosine, and tryptophan, and deamidation of asparagine and glutamine were treated as dynamic modifications, and carbamidomethylation of cysteine was treated as a fixed modification.

Transposon-insertion sequencing (TIS) analysis. TIS was carried out essentially as previously described (59) but using selection plates containing LB medium with As^V 1 mM. In brief, ~600,000 transposon mutants were generated by conjugation of *V. cholerae* C6706 with SM10λ*pir E. coli* carrying the Himar1 suicide transposon vector pSC189 (60). They were collected, and their genomic DNA was pooled and analyzed on a MiSeq benchtop sequencer (Illumina, San Diego, CA). Insertion sites (which included 35% of TA sites) were identified as previously described (59), and significance was determined using Con-ARTIST simulation-based normalization as described (61). Results were visualized using Artemis (62).

As^V resistance screen of arrayed transposon mutant library. A nonredundant transposon insertion library from the *V. cholerae* strain C6706 (63) consisting of 3,156 insertion mutants was used to determine genetic determinants providing resistance to As^V in *V. cholerae*. *V. cholerae* WT and the library insertion mutants were first grown aerobically in 200 μL of LB in 96-well plates at 37°C for 24 h. These cultures were then used as inoculum in 96-well plates containing 200 μL complete LB medium, in the presence of 1 mM As^V. The 96-well plates were incubated under agitation at 37°C for 24 h, and then resistance to As^V was evaluated by measuring the optical density (OD_{600}) using a BioTek Eon plate reader.

Protein homology studies of As^V resistance determinants in enteric pathogens. DNA sequences of the *V. cholerae arsR*, *varG*, *varH*, and *arsJ var* genes and complete genomes sequences of the enteric pathogens *Salmonella* Typhimurium (BioProject no. PRJNA241), *Citrobacter rodentium* (PRJNA261533), *Shigella flexneri* (PRJNA553848), EHEC (PRJNA218110), and *Yersinia pseudotuberculosis* (PRJEB6403) were downloaded from the NCBI database. Complete genomes of the pathogens were translated using Prodigal ver. 2.6.2, and homologous sequences to the *V. cholerae* Var proteins were queried against the enteric pathogens by BLASTP ver. 2.9.0. Sequence homology data were represented in a heatmap diagram with Spearman correlation done with R ver. 3.6.1.

β-Galactosidase activity determination. β-Galactosidase activity was measured through *o*-nitrophenyl-β-D-galactopyranoside (ONPG) cleavage by the product of the *lacZ* reporter gene, and specific activity was calculated in Miller units (64). In brief, cultures of *V. cholerae* carrying the pCB192N plasmid harboring promoter gene insertions (see Table S2) were grown at 37°C overnight in 15-mL Falcon tubes containing 3 mL of LB complete medium. Overnight cultures were diluted 1:200 and supplemented with 1 mM As^V and incubated at 37°C until they reached mid-log phase (OD_{600}, 0.4 to 0.7). Aliquots (100- μL)

TABLE 1 MRM transitions, declustering potentials, and collision energies of metabolites

Analyte	Q1 (m/z)	Q3 (m/z)	DP (V)	CE (V)
3-Phospho glycerate	187.2	98.9	+60	19.2
Ribitol	150.8	88.9	−60	−14.2

of three different subcultures were collected, and cells were permeabilized and assayed in triplicate for each strain as previously described (64).

Determination of intracellular and extracellular As^V and As^{III} in *V. cholerae*. To determinate concentrations of As^V and As^{III} in supernatants of *V. cholerae* and *E. coli*, bacterial cells were grown in the presence of As^V for 5 h and then pelleted. Supernatants of each strain were identified to the species level by high-performance liquid chromatography (HPCL) (Agilent Infinity II 1290) using a C_{18} column reverse-phase method (130 Å, 1.7 μm, 2.1 mm by 150 mm; Waters, USA). The elution conditions used were flow rate, 1 mL min^{-1}; temperature, 25°C; isocratic elution in 5 mM tetrabutylammonium hydroxide, 5% methanol (vol/vol) and 3 mM malonic acid. Identification and quantification of As^V and As^{III} were performed by inductively coupled plasma mass spectroscopy (ICP-MS) (Agilent 8900 ICP-MS Triple Quad) by comparison to standards of known concentration and peak integration.

To determine intracellular concentrations of As^V and As^{III} in *V. cholerae*, the pelleted cells were washed in complete LB medium to remove traces of arsenic and then resuspended in 500 μL of H_2O. Glass beads were adding to the resuspension, and cells were lysed by bead-beating. The resulting extract was centrifuged, and As^V and As^{III} from those supernatants were analyzed by ICP-MS as previously described. Samples were analyzed in triplicate.

LC-MS/MS analysis using the QTRAP 6500+. To measure 3-phosphoglycerate (3PG), *V. cholerae* cells grown in the presence of 5 mM As^V were pelleted and used for LC-MS/MS analysis. Bacterial pellets were resuspended in 1 mL ice-cold 60% ethanol containing 2 μM ribitol as the internal control. The cells were mechanically disrupted using a bead homogenizer set to oscillate for 3 cycles of 30 s each at 6,800 rpm with a 10-s pause between each cycle. Cell debris was separated at 13,000 rpm. An aliquot (200 μL) of the supernatant containing intracellular metabolites was vacuum dried and resuspended in an equal volume of 7.5 mM ammonium bicarbonate solution before LC-MS/MS analysis.

A triple-quadrupole-ion trap hybrid mass spectrometer, QTRAP 6500+ instrument (SCIEX, USA) connected with a Waters ultraperformance liquid chromatography (UPLC) I-class system was used for metabolite analysis. The chromatographic separation was performed on an XSELECT HSS XP column (150 mm by 2.1 mm inside diameter [i.d.]; 2.5 μm particle size; Waters, USA) using a binary solvent system at a flow rate of 0.1 mL/min. Mobile phase A was composed of 7.5 mM ammonium bicarbonate in LC-MS-grade water, and mobile phase B was 100% LC-MS grade methanol. The column was maintained at 40°C, and the autosampler temperature was set to 7°C. The A/B solvent ratio was maintained at 100/0 for 2 min, followed by a gradual increase of solvent B to 95% for 2 min. The solvent B was maintained at 95% over the next 5 min. The gradient was reduced to 100% solvent A within 0.5 min, and the column was equilibrated for 5.5 min before the next run. The needle was washed with 1.2 mL of a strong wash solution containing 100% LC-MS-grade acetonitrile followed by 1 mL of a weak wash solution composed of 10% aqueous methanol before each injection. The injection volume was 5 μL. The QTRAP 6500+ (SCIEX) was operated in negative as well as positive ion mode for targeted quantitation in multiple reaction monitoring (MRM). MRM parameters for each analyte are listed in Table 1. The electrospray ionization (ESI) parameters used are as follows: electrospray ion voltage of −4,500 V in negative and 5,500 V in positive mode, source temperature of 400°C, curtain gas of 35, and gas 1 and 2 of 40 lb/in^2 each. The compound-specific parameters, such as declustering potential (DP) and collision energy (CE), were optimized for each compound using manual tuning. These values are listed in Table 1.

Detection of 1As3PG. 1As3PG was identified using a Thermo Orbitrap Exploris 480 high-resolution mass spectrometer. The chromatographic method used for this analysis was the same as that described for the LC-MS/MS performed using the QTRAP6500+. The MS data were acquired in both positive and negative polarity within mass range of 140 to 400 Da. The precursor ion resolution was maintained at 240,000, whereas the product ion resolution was maintained at 120,000. Deprotonated $[M\text{-}H]^-$ ion of 1As3PG was detected at *m/z* 304.8696 Da compared to the actual mass of 304.8674 Da; thus, $\Delta m = 7.149$ ppm. The fragmentation pattern of 1As3PG could not be further resolved under these conditions.

Protein structural and topological analysis. Protein alignments were performed by using Vector NTI. Prediction of the VarH secondary structure was performed by using Phyre2 (http://www.sbg.bio.ic.ac.uk/phyre2/html/page.cgi?id=index). Structural prediction of the VarG and VarH proteins was performed with AlphaFold2 on the CoLabFold publicly accessible interface (65) (https://colab.research.google.com/github/sokrypton/ColabFold/blob/main/AlphaFold2.ipynb). Sequences were modeled as monomers using mmseqs2 for multiple sequence alignment. Studies on protein topological similarity were carried out by using TM-score (https://zhanggroup.org/TM-score/).

Competition assays. Aerobic overnight cultures of *V. cholerae* C6706 wild-type *lacZ*$^-$ and enterohemorrhagic *Escherichia coli* EHEC O157:H7 *lacZ*$^+$, *Salmonella enterica* serovar Typhimurium *LT2 lacZ*$^+$, *Citrobacter rodentium* DBS100 *lacZ*$^+$, *Shigella flexneri* M90T *lacZ*$^+$, and *Yersinia pseudotuberculosis* YPIII *lacZ*$^+$ were collected, and 1×10^7 cells were coinoculated at a 1:1 ratio in 15-mL tubes containing 3 mL of complete LB medium without or with 10 mM As^V. After 8 h of incubation at 37°C, an aliquot was diluted and plated on LB agar plates containing X-Gal (5-bromo-4-chloro-3-indolyl-β-D-galactopyranoside) to enumerate wild-type and competing strains. Competitive indices (CIs) were determined by

dividing the ratio mutant or non-WT strain to C6706 wild-type colonies by the ratio in the inoculum. To calculate CIs among *V. cholerae* strain C6706 against a different *V. cholerae* strain against enteric pathogens (Fig. 1B), CIs obtained after the As^V challenge were normalized to the respective CIs obtained after competition in the absence of As^V.

***In vitro* GAPDH and phosphatase enzymatic assays.** The GAPDH activity assay was performed in accordance with the manufacturer's instructions (MAK27; Sigma-Aldrich) but using P_i or As^V as the GAPDH substrate; 10 μg of purified *V. cholerae* VarG and VC2000 enzymes were used in the assay. This assay quantifies GAPDH activity by measuring enzymes' capacity to reduce NAD^+ to NADH during the conversion of glyceraldehyde 3-phosphate to 1,3-biphosphoglycerate. The NADH produced in this reaction results in a colorimetric (OD_{450}) product proportional to the GAPDH activity of the enzyme. GAPDH activity is reported as nmol/min/mL = milliunit/mL. One unit of GAPDH is the amount of enzyme that will generate 1.0 mmol of NADH per minute at pH 7.2 at 37°C.

Phosphatase activity was quantified using Cayman's phosphatase colorimetric assay kit and 5 μg of purified *V. cholerae* VarH, C113G R119G VarH, VC1041 (positive control), and BsrV (negative control) enzymes. The assay uses *p*-nitrophenylphosphate (pNPP) as the substrate for phosphatase enzymes. Phosphatase enzymes dephosphorylate pNPP, which deprotonates its phenolic OH-group by increasing the pH of the reaction; deprotonated pNP yields an intense yellow color detected at OD 405 nm. Enzymatic activities were calculated as μmol of phosphate released per min/mL.

Flow cytometry analysis. *V. cholerae* WT and the indicated *var* mutant strains were grown for 5 h in the presence of 1 mM As^V, and then aliquots (1 mL) from each culture were pelleted, washed once, and resuspended in PBS (100 μL) to measure membrane potential and ROS.

To measure membrane potential in *V. cholerae* cells, we used the BacLight bacterial membrane potential kit (Invitrogen). *V. cholerae* samples resuspended in 100 μL PBS were incubated for 15 min at 20°C in the dark with the dye 30 μM 3,3′-diethyloxacarbocyanine iodide ($DiOC_2$). Next, cells were washed twice with PBS and resuspended in 2 mL of PBS, and then the fluorescence emitted from treated cells was measured with a Bio-Rad S3e cell sorter at an excitation wavelength of 488 nm and an emission wavelength of 525/30 nm (for green) or 655 nm (for red).

ROS measurements were performed using the CellROX green reagent for oxidative stress detection (Thermo Fisher). Washed *V. cholerae* cells were supplemented with CellROX reagent at a final concentration of 5 μM and were incubated for 30 min at 37°C. Next, cells were washed twice with PBS and resuspended in 2 mL of PBS, and then the fluorescence emitted was measured with a Bio-Rad S3e cell sorter at an excitation wavelength of 488 nm and an emission wavelength of 525 nm.

Data availability. The TIS raw data can be found at https://data.mendeley.com/datasets/kj9xxffpc7/1. A table showing underrepresented genes found by TIS can be found at https://data.mendeley.com/datasets/c64h244vs8/2. Proteomic and TPP raw data can be found at http://www.ebi.ac.uk/pride/archive/projects/PXD035237 and ftp://ftp.pride.ebi.ac.uk/pride/data/archive/2022/07/PXD035237. A table showing TPP targets can be found at https://data.mendeley.com/datasets/rhp3fs33yy/2.

Statistics and reproducibility. Statistical significance was assessed with Student's *t* test where indicated. A *P* value of less than 0.05 was considered statistically significant. Assays were performed with three biological replicates unless otherwise indicated.

SUPPLEMENTAL MATERIAL

Supplemental material is available online only.

FIG S1, TIF file, 0.1 MB.
FIG S2, TIF file, 2.3 MB.
FIG S3, TIF file, 0.2 MB.
FIG S4, TIF file, 2.7 MB.
FIG S5, TIF file, 1.1 MB.
FIG S6, TIF file, 2.7 MB.
FIG S7, TIF file, 1.9 MB.
TABLE S1, DOCX file, 0.01 MB.
TABLE S2, DOCX file, 0.03 MB.
TABLE S3, DOCX file, 0.01 MB.

ACKNOWLEDGMENTS

This work was supported by the Knut and Alice Wallenberg Foundation (KAW), The Laboratory of Molecular Infection Medicine Sweden (MIMS), the Swedish Research Council, and the Kempe Foundation. V.C.T. and D.D.S. were supported by the National Institutes of Health/National Institute of Allergy and Infectious Diseases (NIH/NIAID) grants P01-AI83211 (Metabolomics Core) and R01-AI125588.

The metabolomics analyses were performed at the University of Nebraska Medical Center Mass Spectrometry and Proteomics Core Facility administered through the Office of the Vice Chancellor for Research and supported by state funds from the Nebraska Research Initiative (NRI). We thank Erik Björk and Laurent Ouerdane for their

help with the ICPMS analyses and for insightful discussions, J. J. Mekalanos for the *V. cholerae* C6706 Transposon-mutant library, and Inigo Ruiz and David Arranz for their technical support.

We declare that there are no competing interests in relation with the work described.

REFERENCES

1. Kalia K, Joshi DN. 2009. Detoxification of arsenic, p 1083–1100. *In* Gupta RC, Handbook of toxicology of chemical warfare agents. Academic Press, San Diego, CA.
2. Singh R, Singh S, Parihar P, Singh VP, Prasad SM. 2015. Arsenic contamination, consequences and remediation techniques: a review. Ecotoxicol Environ Saf 112:247–270. https://doi.org/10.1016/j.ecoenv.2014.10.009.
3. Pal C, Asiani K, Arya S, Rensing C, Stekel DJ, Larsson DGJ, Hobman JL. 2017. Metal resistance and its association with antibiotic resistance. Adv Microb Physiol 70:261–313. https://doi.org/10.1016/bs.ampbs.2017.02.001.
4. Hobman JL, Crossman LC. 2015. Bacterial antimicrobial metal ion resistance. J Med Microbiol 64:471–497. https://doi.org/10.1099/jmm.0.023036-0.
5. Willsky GR, Malamy MH. 1980. Characterization of two genetically separable inorganic phosphate transport systems in Escherichia coli. J Bacteriol 144:356–365. https://doi.org/10.1128/jb.144.1.356-365.1980.
6. Willsky GR, Malamy MH. 1980. Effect of arsenate on inorganic phosphate transport in Escherichia coli. J Bacteriol 144:366–374. https://doi.org/10.1128/jb.144.1.366-374.1980.
7. Dixon HBF. 1996. The biochemical action of arsonic acids especially as phosphate analogues. Adv Inorg Chem 44:191–227. https://doi.org/10.1016/S0898-8838(08)60131-2.
8. Rosen BP. 2002. Biochemistry of arsenic detoxification. FEBS Lett 529:86–92. https://doi.org/10.1016/s0014-5793(02)03186-1.
9. Yang HC, Fu HL, Lin YF, Rosen BP. 2012. Pathways of arsenic uptake and efflux. Curr Top Membr 6:325–358. https://doi.org/10.1016/B978-0-12-394390-3.00012-4.
10. Scott N, Hatlelid KM, MacKenzie NE, Carter DE. 1993. Reactions of arsenic (III) and arsenic (V) species with glutathione. Chem Res Toxicol 6:102–106. https://doi.org/10.1021/tx00031a016.
11. Przygoda G, Feldmann J, Cullen WR. 2001. The arsenic eaters of Styria: a different picture of people who were chronically exposed to arsenic. Appl Organometal Chem 15:457–462. https://doi.org/10.1002/aoc.126.
12. Liu J, Lu Y, Wu Q, Goyer R a, Waalkes MP. 2008. Mineral arsenicals in traditional medicines: orpiment, realgar, and arsenolite. J Pharmacol Exp Ther 326:363–368. https://doi.org/10.1124/jpet.108.139543.
13. Shahpiri A, Mohammadzadeh A. 2018. Bioaccumulation of arsenic by engineered Escherichia coli cells expressing rice metallothionein isoforms. Curr Microbiol 75:1537–1542. https://doi.org/10.1007/s00284-018-1556-3.
14. Thomas DJ, Rosen BP. 2013. Arsenic methyltransferases, p 138–143. *In* Kretsinger RH, Uversky VN, Permyakov EA (ed), Encyclopedia of metalloproteins. Springer, New York, NY.
15. Saltikov CW, Newman DK. 2003. Genetic identification of a respiratory arsenate reductase. Proc Natl Acad Sci U S A 100:10983–10988. https://doi.org/10.1073/pnas.1834303100.
16. Oden KL, Gladysheva TB, Rosen BP. 1994. Arsenate reduction mediated by the plasmid-encoded ArsC protein is coupled to glutathione. Mol Microbiol 12:301–306. https://doi.org/10.1111/j.1365-2958.1994.tb01018.x.
17. Chen J, Yoshinaga M, Garbinski LD, Rosen BP. 2016. Synergistic interaction of glyceraldehydes-3-phosphate dehydrogenase and ArsJ, a novel organoarsenical efflux permease, confers arsenate resistance. Mol Microbiol 100:945–953. https://doi.org/10.1111/mmi.13371.
18. Wu S, Wang L, Gan R, Tong T, Bian H, Li Z, Du S, Deng Z, Chen S. 2018. Signature arsenic detoxification pathways in Halomonas sp. Strain GFAJ-1. mBio 9:e00515-18. https://doi.org/10.1128/mBio.00515-18.
19. Ben Fekih I, Zhang C, Li YP, Zhao Y, Alwathnani HA, Saquib Q, Rensing C, Cervantes C. 2018. Distribution of arsenic resistance genes in prokaryotes. Front Microbiol 9:2473. https://doi.org/10.3389/fmicb.2018.02473.
20. Németi B, Anderson ME, Gregus Z. 2012. Glutathione synthetase promotes the reduction of arsenate via arsenolysis of glutathione. Biochimie 94:1327–1333. https://doi.org/10.1016/j.biochi.2012.02.033.
21. Demel S, Shi JIN, Martin P, Rosen BP, Edwards BFP. 2004. Arginine 60 in the ArsC arsenate reductase of E. coli plasmid R773 determines the chemical nature of the bound As(III) product. Protein Sci 13:2330–2340. https://doi.org/10.1110/ps.04787204.
22. Martin P, Demel S, Shi J, Gladysheva T, Gatti DL, Rosen BP, Edwards BFP. 2001. Insights into the structure, solvation, and mechanism of ArsC arsenate reductase, a novel arsenic detoxification enzyme. Structure 9:1071–1081. https://doi.org/10.1016/S0969-2126(01)00672-4.
23. Heidelberg JF, Eisen JA, Nelson WC, Clayton RA, Gwinn ML, Dodson RJ, Haft DH, Hickey EK, Peterson JD, Umayam L, Gill SR, Nelson KE, Read TD, Tettelin H, Richardson D, Ermolaeva MD, Vamathevan J, Bass S, Qin H, Dragoi I, Sellers P, McDonald L, Utterback T, Fleishmann RD, Nierman WC, White O, Salzberg SL, Smith HO, Colwell RR, Mekalanos JJ, Venter JC, Fraser CM. 2000. DNA sequence of both chromosomes of the cholera pathogen Vibrio cholerae. Nature 406:477–483. https://doi.org/10.1038/35020000.
24. Jenkins JL, Tanner JJ. 2006. High-resolution structure of human D-glyceraldehyde-3-phosphate dehydrogenase. Acta Crystallogr D Biol Crystallogr 62:290–301. https://doi.org/10.1107/S0907444905042289.
25. Velick SF. 1955. Glyceraldehyde-3-phosphate dehydrogenase from muscle. Methods Enzymol 1:401–406. https://doi.org/10.1016/0076-6879(55)01065-3.
26. Gregus Z, Németi B. 2005. The glycolytic enzyme glyceraldehyde-3-phosphate dehydrogenase works as an arsenate reductase in human red blood cells and rat liver cytosol. Toxicol Sci 85:859–869. https://doi.org/10.1093/toxsci/kfi158.
27. Byers LD, She HS, Alayoff A. 1979. Interaction of phosphate analogues with glyceraldehyde-3-phosphate dehydrogenase. Biochemistry 18:2471–2480. https://doi.org/10.1021/bi00579a006.
28. Aoyama K, Nakaki T. 2015. Glutathione in cellular redox homeostasis: association with the excitatory amino acid carrier 1 (EAAC1). Molecules 20:8742–8758. https://doi.org/10.3390/molecules20058742.
29. Wang H, Naseer N, Chen Y, Zhu AY, Kuai X, Galagedera N, Liu Z, Zhu J. 2017. OxyR2 modulates OxyR1 activity and Vibrio cholerae oxidative stress response. Infect Immun 85:e00929-16. https://doi.org/10.1128/IAI.00929-16.
30. Mateus A, Kurzawa N, Becher I, Sridharan S, Helm D, Stein F, Typas A, Savitski MM. 2020. Thermal proteome profiling for interrogating protein interactions. Mol Syst Biol 16:1–11. https://doi.org/10.15252/msb.20199232.
31. Nordstrom DK. 2002. Worldwide occurrences of arsenic in ground water. Science 296:2143–2145. https://doi.org/10.1126/science.1072375.
32. Joel P, Michael B. 2020. Global threat of arsenic in groundwater. Science 850:845–850. https://doi.org/10.1126/science.aba1510.
33. Jin Q, Yuan Z, Xu J, Wang Y, Shen Y, Lu W, Wang J, Liu H, Yang J, Yang F, Zhang X, Zhang J, Yang G, Wu H, Qu D, Dong J, Sun L, Xue Y, Zhao A, Gao Y, Zhu J, Kan B, Ding K, Chen S, Cheng H, Yao Z, He B, Chen R, Ma D, Qiang B, Wen Y, Hou Y, Yu J. 2002. Genome sequence of Shigella flexneri 2a: insights into pathogenicity through comparison with genomes of Escherichia coli K12 and O157. Nucleic Acids Res 30:4432–4441. https://doi.org/10.1093/nar/gkf566.
34. Batzilla J, Höper D, Antonenka U, Heesemann J, Rakin A. 2011. Complete genome sequence of Yersinia enterocolitica subsp. palearctica serogroup O:3. J Bacteriol 193:2067. https://doi.org/10.1128/JB.01484-10.
35. Pearson BM, Gaskin DJH, Segers RPAM, Wells JM, Nuijten PJM, Van Vliet AHM. 2007. The complete genome sequence of Campylobacter jejuni strain 81116 (NCTC11828). J Bacteriol 189:8402–8403. https://doi.org/10.1128/JB.01404-07.
36. McClelland M, Xie Y, Sanderson KE, Spieth J, Clifton SW, Latreille P, Courtney L, Porwollik S, Ali J, Dante M, Du F, Hou S, Layman D, Leonard S, Nguyen C, Scott K, Holmes A, Grewal N, Mulvaney E, Ryan E, SUN H, Florea L, Miller W, Stoneking T, Nhan M, Waterston R, Wilson RK. 2001. Complete genome sequence of Salmonella enterica serovar Typhimurium LT2. Nature 413:852–856.
37. Popov G, Fiebig-Comyn A, Shideler S, Coombes BK, Savchenko A. 2019. Complete genome sequence of Citrobacter rodentium strain DBS100. Microbiol Resour Announc 8:e00421-19. https://doi.org/10.1128/MRA.00421-19.

38. Shi W, Wu J, Rosen BP. 1994. Identification of a putative metal binding site in a new family of metalloregulatory proteins. J Biol Chem 269:19826–19829. https://doi.org/10.1016/S0021-9258(17)32094-X.
39. Sirover MA. 2011. On the functional diversity of glyceraldehyde-3-phosphate dehydrogenase: biochemical mechanisms and regulatory control. Biochim Biophys Acta 1810:741–751. https://doi.org/10.1016/j.bbagen.2011.05.010.
40. Ferreira E, Giménez R, Alexandra M, Aguilera L, Aguilar J, Badia J, Baldomà L. 2015. Glyceraldehyde-3-phosphate dehydrogenase is required for efficient repair of cytotoxic DNA lesions in Escherichia coli. Int J Biochem Cell Biol 60:202–212. https://doi.org/10.1016/j.biocel.2015.01.008.
41. Whitworth DE, Morgan BH. 2015. Synergism between bacterial GAPDH and OMVs: disparate mechanisms but co-operative action. Front Microbiol 6:1231. https://doi.org/10.3389/fmicb.2015.01231.
42. Leveson-Gower RB, Mayer C, Roelfes G. 2019. The importance of catalytic promiscuity for enzyme design and evolution. Nat Rev Chem 3:687–705. https://doi.org/10.1038/s41570-019-0143-x.
43. Shi H, Shi X, Liu KJ. 2004. Oxidative mechanism of arsenic toxicity and carcinogenesis. Mol Cell Biochem 255:67–78. https://doi.org/10.1023/B:MCBI.0000007262.26044.e8.
44. Liu SX, Athar M, Lippai I, Waldren C, Hei TK. 2001. Induction of oxyradicals by arsenic: implication for mechanism of genotoxicity. Proc Natl Acad Sci U S A 98:1643–1648. https://doi.org/10.1073/pnas.98.4.1643.
45. Sukchawalit R, Prapagdee B, Charoenlap N, Vattanaviboon P, Mongkolsuk S. 2005. Protection of Xanthomonas against arsenic toxicity involves the peroxide-sensing transcription regulator OxyR. Res Microbiol 156:30–34. https://doi.org/10.1016/j.resmic.2004.07.005.
46. Wang H, Chen S, Zhang J, Rothenbacher FP, Jiang T, Kan B, Zhong Z, Zhu J. 2012. Catalases promote resistance of oxidative stress in Vibrio cholerae. PLoS One 7:e53383. https://doi.org/10.1371/journal.pone.0053383.
47. Miki H, Funato Y. 2012. Regulation of intracellular signalling through cysteine oxidation by reactive oxygen species. J Biochem 151:255–261. https://doi.org/10.1093/jb/mvs006.
48. Mondal P, Majumder CB, Mohanty B. 2006. Laboratory based approaches for arsenic remediation from contaminated water: recent developments. J Hazard Mater 137:464–479. https://doi.org/10.1016/j.jhazmat.2006.02.023.
49. Brammer H. 2008. Threat of arsenic to agriculture in India, Bangladesh and Nepal. Econ Polit Wkly 43:79–84.
50. Coryell M, McAlpine M, Pinkham NV, McDermott TR, Walk ST. 2018. The gut microbiome is required for full protection against acute arsenic toxicity in mouse models. Nat Commun 9:1–9. https://doi.org/10.1038/s41467-018-07803-9.
51. Baba T, Ara T, Hasegawa M, Takai Y, Okumura Y, Baba M, Datsenko KA, Tomita M, Wanner BL, Mori H. 2006. Construction of Escherichia coli K-12 in-frame, single-gene knockout mutants: the Keio collection. Mol Syst Biol 2:1–11. https://doi.org/10.1038/msb4100050.
52. Donnenberg MS, Kaper JB. 1991. Construction of an eae deletion mutant of enteropathogenic Escherichia coli by using a positive-selection suicide vector. Infect Immun 59:4310–4317. https://doi.org/10.1128/iai.59.12.4310-4317.1991.
53. Guzman LM, Belin D, Carson MJ, Beckwith J. 1995. Tight regulation, modulation, and high-level expression by vectors containing the arabinose PBAD promoter. J Bacteriol 177:4121–4130. https://doi.org/10.1128/jb.177.14.4121-4130.1995.
54. Schneider K, Beck CF. 1986. Promoter-probe vectors for the analysis of divergently arranged promoters. Gene 42:37–48. https://doi.org/10.1016/0378-1119(86)90148-4.
55. Mateus A, Hevler J, Bobonis J, Kurzawa N, Shah M, Mitosch K, Goemans CV, Helm D, Stein F, Typas A, Savitski MM. 2020. The functional proteome landscape of Escherichia coli. Nature 588:473–478. https://doi.org/10.1038/s41586-020-3002-5.
56. Hughes CS, Moggridge S, Müller T, Sorensen PH, Morin GB, Krijgsveld J. 2019. Single-pot, solid-phase-enhanced sample preparation for proteomics experiments. Nat Protoc 14:68–85. https://doi.org/10.1038/s41596-018-0082-x.
57. Franken H, Mathieson T, Childs D, Sweetman GMA, Werner T, Tögel I, Doce C, Gade S, Bantscheff M, Drewes G, Reinhard FBM, Huber W, Savitski MM. 2015. Thermal proteome profiling for unbiased identification of direct and indirect drug targets using multiplexed quantitative mass spectrometry. Nat Protoc 10:1567–1593. https://doi.org/10.1038/nprot.2015.101.
58. Ritchie ME, Phipson B, Wu D, Hu Y, Law CW, Shi W, Smyth GK. 2015. Limma powers differential expression analyses for RNA-sequencing and microarray studies. Nucleic Acids Res 43:e47. https://doi.org/10.1093/nar/gkv007.
59. Chao MC, Pritchard JR, Zhang YJ, Rubin EJ, Livny J, Davis BM, Waldor MK. 2013. High-resolution definition of the Vibrio cholerae essential gene set with hidden Markov model-based analyses of transposon-insertion sequencing data. Nucleic Acids Res 41:9033–9048. https://doi.org/10.1093/nar/gkt654.
60. Chiang SL, Rubin EJ. 2002. Construction of a mariner-based transposon for epitope-tagging and genomic targeting. Gene 296:179–185. https://doi.org/10.1016/s0378-1119(02)00856-9.
61. Pritchard JR, Chao MC, Abel S, Davis BM, Baranowski C, Zhang YJ, Rubin EJ, Waldor MK. 2014. ARTIST: high-resolution genome-wide assessment of fitness using transposon-insertion sequencing. PLoS Genet 10:e1004782. https://doi.org/10.1371/journal.pgen.1004782.
62. Carver T, Harris SR, Berriman M, Parkhill J, McQuillan JA. 2012. Artemis: an integrated platform for visualization and analysis of high-throughput sequence-based experimental data. Bioinformatics 28:464–469. https://doi.org/10.1093/bioinformatics/btr703.
63. Cameron DE, Urbach JM, Mekalanos JJ. 2008. A defined transposon mutant library and its use in identifying motility genes in Vibrio cholerae. Proc Natl Acad Sci U S A 105:8736–8741. https://doi.org/10.1073/pnas.0803281105.
64. Miller JH. 1972. Experiments in molecular genetics. Cold Spring Harbor Laboratory, Cold Spring Harbor, NY.
65. Jumper J, Evans R, Pritzel A, Green T, Figurnov M, Ronneberger O, Tunyasuvunakool K, Bates R, Žídek A, Potapenko A, Bridgland A, Meyer C, Kohl SAA, Ballard AJ, Cowie A, Romera-Paredes B, Nikolov S, Jain R, Adler J, Back T, Petersen S, Reiman D, Clancy E, Zielinski M, Steinegger M, Pacholska M, Berghammer T, Bodenstein S, Silver D, Vinyals O, Senior AW, Kavukcuoglu K, Kohli P, Hassabis D. 2021. Highly accurate protein structure prediction with AlphaFold. Nature 596:583–589. https://doi.org/10.1038/s41586-021-03819-2.